CONCLUSION

Decreased BMIPP uptake relative to thallium perfusion was often seen at rest in patients with coronary artery disease without myocardial infarction. This decreased BMIPP uptake is probably a result of prolonged and severe myocardial ischemia which is often associated with regional wall motion abnormality.

REFERENCES

1. Neely JR, Rovetto M, Oran J. Myocardial utilization of carbohydrate and lipids. *Prog Cardiovasc Dis* 1972;15:289–329.
2. Liedke AJ. Alterations of carbohydrate and lipid metabolism in the acutely ischemic heart. *Prog Cardiovasc Dis* 1981;23:321–336.
3. Vanoverschelde JL, Wijns W, Depre C, et al. Mechanisms of chronic regional postischemic dysfunction in humans: new insight from the study of noninfarcted collateral-dependent myocardium. *Circulation* 1993;87:1513–1523.
4. Rahimtoola SH. The hibernating myocardium. *Am Heart J* 1989;117:211–221.
5. Braunwald E, Kloner RA. The stunned myocardium: prolonged, postischemic ventricular dysfunction. *Circulation* 1982;60:1146–1149.
6. Braunwald E, Rutherford JD. Reversible ischemic left ventricular dysfunction: evidence for hibernating myocardium. *J Am Coll Cardiol* 1986;8:1467–1470.
7. Bolli R. Myocardial stunning in man. *Circulation* 1992;86:1671–1691.
8. Knabb RM, Bergmann SR, Fox KAA, Sobel BE. The temporal pattern of recovery of myocardial perfusion and metabolism delineated by positron emission tomography after coronary thrombolysis. *J Nucl Med* 1987;28:1563–1570.
9. Schwaiger M, Schelbert HR, Ellison D, et al. Sustained regional abnormalities in cardiac metabolism after transient ischemia in the chronic dog model. *J Am Coll Cardiol* 1985;5:336–347.
10. Knapp FF Jr, Knopp J. Iodine-123-labeled fatty acids for myocardial single-photon emission tomography: current status and future perspectives. *Eur J Nucl Med* 1995;22:361–381.
11. Knapp FF Jr, Kropp J, Goodman MM, et al. The development of iodine-123 methyl-branched fatty acids and their applications in nuclear cardiology. *Ann Nucl Med* 1993;7:1–14.
12. Goodman MM, Kirsch G, Knapp FF Jr. Synthesis and evaluation of radioiodinated terminal p-iodophenyl-substituted α- and β-methyl-branched fatty acids. *J Med Chem* 1984;27:390–397.
13. Knapp FF Jr, Ambrose KR, Goodman MM. New radioiodinated methyl-branched fatty acids for cardiac imaging. *Eur J Nucl Med* 1986;12:45–48.
14. Braunwald E. Unstable angina. A classification. *Circulation* 1989;80:410–414.
15. Yonekura Y, Brill AB, Som P, et al. Regional myocardial substrate uptake in hypertensive rats: a quantitative autoradiographic measurement. *Science* 1985;227: 1494–1496.
16. Yamamoto K, Som P, Brill AB, et al. Dual-tracer autoradiographic study of beta-methyl (^{14}C-I) heptadecanoic acid and 15-p-(^{131}I)-iodophenyl-beta-methyl pentadecanoic acid in normotensive and hypertensive rats. *J Nucl Med* 1986;27:1178–1183.
17. Nishimura T, Sago M, Kihara K. Fatty acid myocardial imaging using ^{123}I-β-methyl-iodophenyl pentadecanoic acid (BMIPP): comparison of myocardial perfusion and fatty acid utilization in canine myocardial infarction (occlusion and reperfusion model). *Eur J Nucl Med* 1989;15:341–345.
18. Miller DD, Gill JB, Elmaleh D, Arez T, Boucher CA, Strauss HW. Fatty acid analogue accumulation: a marker of myocite viability in ischemic-reperfused myocardium. *Circ Res* 1988;63:681–692.
19. Kawamoto M, Tamaki N, Yonekura Y, et al. Significance of myocardial uptake of iodine-123-labeled beta-methyl iodophenyl pentadecanoic acid: comparison with kinetics of carbon-11-labeled palmitate. *J Nucl Cardiol* 1994;1:522–528.
20. Saito S, Yasuda T, Gold HK, et al. Differentiation of regional perfusion and fatty acid uptake in zones of myocardial injury. *Nucl Med Commun* 1991;12:663–675.
21. Tamaki N, Kawamoto M, Yonekura Y, et al. Regional metabolic abnormality in relation to perfusion and wall motion in patients with myocardial infarction: assessment with emission tomography using an iodinated branched fatty acid analog. *J Nucl Med* 1992;33:659–667.
22. De Geeter F, Franken PR, Knapp FF Jr, Bossuyt A. Relationship between blood flow and fatty acid metabolism in subacute myocardial infarction: a study by means to technetium-99m-MIBI and iodine-123-beta-methyl iodophenyl pentadecanoic acid. *Eur J Nucl Med* 1994;21:283–291.
23. Franken PR, Demoor D, De Dadeleer C, Block P, Bossuyt A. Abnormal free fatty acid uptake in subacute myocardial infarction after coronary thrombolysis: correlation with wall motion and inotropic reserve. *J Nucl Med* 1994;35:1758–1765.
24. Tamaki N, Kawamoto M, Yonekura Y, et al. Assessment of fatty acid metabolism using iodine-123 branched fatty acid: comparison with positron emission tomography. *Ann Nucl Med* 1993;7:41–48.
25. Tamaki N, Kawamoto M. The use of iodinated free fatty acids for assessing fatty acid metabolism. *J Nucl Cardiol* 1994;1:72–78.
26. Kawamoto M, Tamaki N, Yonekura Y, et al. Combined study with iodine-123 fatty acid and ^{201}Tl to assess ischemic myocardium: comparison with thallium redistribution and glucose metabolism. *Ann Nucl Med* 1994;8:847–854.
27. Di-Carli M, Czernin J, Hoh CK, et al. Relation among stenosis severity, myocardial blood flow and flow reserve in patients with coronary artery disease. *Circulation* 1995;91:1944–1951.
28. Uren NG, Melin JA, De Bruyne B, Wijins W, Baudhuin T, Camici PG. Relation between myocardial blood flow and the severity of coronary-artery stenosis. *N Engl J Med* 1994;330:1782–1788.
29. Schwaiger M, Schelbert HR, Keen R, et al. Retention and clearance of ^{11}C palmitic acid in ischemic and reperfused canine myocardium. *J Am Coll Cardiol* 1985;6:311–320.

Regional Abnormality of Iodine-123-MIBG in Diabetic Hearts

Naoya Hattori, Nagara Tamaki, Tatsuya Hayashi, Izuru Masuda, Takashi Kudoh, Madoka Tateno, Eiji Tadamura, Yoshiharu Yonekura, Kazuwa Nakao and Junji Konishi

Department of Nuclear Medicine and Department of Medicine and Clinical Science, Kyoto University Faculty of Medicine, Kyoto, Japan; and Biomedical Imaging Research Center, Fukui Medical School, Fukui, Japan

Autonomic neuropathy along with cardiac denervation is one of the prognostic factors of diabetic patients. The aim of this study was to establish qualitative and quantitative assessment of diabetic cardiac denervation using [^{123}I]metaiodobenzylguanidine (MIBG). **Methods:** The study population consisted of 31 diabetic patients and 12 control subjects (C). Diabetic patients were classified into the following three groups according to their presentation of neuropathy: N0, without neuropathy; N1, mild neuropathy; N2, severe neuropathy. All subjects underwent triple-phase MIBG scanning, including dynamic planar imaging as well as early and delayed planar and SPECT imaging. Myocardial uptake ratios of MIBG and heart-to-mediastinum count ratios (H/M) were calculated as global uptake indices. Inferior-to-anterior count ratios and coefficients of variation were calculated as regional distribution indices. The washout rate of the inferior wall and whole myocardium were also studied. **Results:** MIBG abnormalities were obvious in the inferior wall, which gradually spread to the adjacent segments. All indices of regional uptake showed a significant difference ($p < 0.01$) among the groups, while only the H/M of the late image showed significant differences in the two global uptake indices ($p = 0.02$). The washout rate of the inferior wall was enhanced with neuropathy. **Conclusion:** Diabetic neuropathy involves an MIBG abnormality in its early stages. Since this abnormality occurs in the inferior segment, an inferior-to-anterior count ratio, an index of regional MIBG uptake could be suitable for the evaluation of this condition because of its superior sensitivity.

Key Words: diabetes; autonomic neuropathy; iodine-123-MIBG

J Nucl Med 1996; 37:1985–1990

Autonomic neuropathy is one of the significant prognostic factors for diabetic patients (*1*). Among these factors, cardiac denervation appears to be a major risk factor of sudden death (*2,3*). Autonomic neuropathy is usually assessed by physical examination (*3–5*) or spectral analysis of heart rate variability (*6,7*).

Received Oct. 30, 1995; revision accepted Apr. 3, 1996.

For correspondence or reprints contact: Naoya Hattori, MD, Department of Nuclear Medicine, Kyoto University, Faculty of Medicine, Shogoin, Sakyo, Kyoto, 606 Japan.

Recently, [^{123}I]metaiodobenzylguanidine (MIBG), a radiolabeled analog of norepinephrine (*8*), was introduced to visualize denervation of the heart. Previous studies using this radiotracer have reported cardiac denervation in advanced diabetes with autonomic neuropathy (*9–11*). However, it still remains unclear whether diabetic neuropathy involves cardiac denervation in its early stages and how cardiac denervation progresses with the diabetes. The aim of the present study was to establish qualitative and quantitative assessments of diabetic cardiac denervation using [^{123}I]MIBG.

MATERIALS AND METHODS

Study Population

We studied 48 diabetic patients. To exclude coronary artery disease and cardiac dysfunction other than diabetic cardiac damage, every patient underwent stress ECG, cardiac ultrasonography, first-pass radionuclide angiography and perfusion SPECT imaging with ^{99m}Tc-tetrofosmin within 1 wk of the MIBG test. To investigate the effects of diabetic damage alone, we excluded patients with cardiac failure, tuberculosis, ischemic heart disease, arterial fibrillation with hypertensive cardiomyopathy and adult T-cell leukemia from the study. We also excluded insulin-dependent diabetes mellitus (IDDM) patients and patients under 30 or over 70 yr old to exclude age-related MIBG reduction (*12,13*). After excluding 17 patients, the study population consisted of 31 patients with noninsulin-dependent diabetes mellitus (NIDDM), 17 men and 14 women, aged 35–69 yr (mean age = 54.3 yr), as summarized in Table 1. A control group of 12 age-matched normal subjects, including 8 men and 4 women (mean age = 53.5 yr), were studied in an identical fashion.

Patient Classification

Diabetic patients were classified into three groups according to their presentation of diabetic neuropathy (*14*) based on Achilles tendon reflex, vibratory sensation and orthostatic hypotension with head-up tilt of 60°: N0 = diabetic patients without neuropathy; N1 = diabetic patients with mild neuropathy, manifesting abnormality in one or two of the tests above; N2 = diabetic patients with severe neuropathy, manifesting abnormality in all the tests. The control group was classified as Group C (Table 1).

Imaging Protocol

SPECT and planar imaging were performed with a triple-head gamma camera system equipped with low-energy, general, all-purpose, parallel-hole collimators. Subjects underwent triple-phase MIBG imaging, including dynamic, early and late scanning. Each patient remained in the resting state throughout the study. Approximately 120 MBq MIBG were injected. At the time of injection, dynamic planar images (0.5 sec per frame) were obtained in the anterior view for 45 sec (dynamic phase). Twenty minutes (early phase) and 4 hr (late phase) after injection, a 3-min planar scan in the anterior view was obtained, after which a 20-min SPECT image was obtained .

During SPECT acquisition, 60 projection images (20 steps × 3) were obtained as 64 × 64 matrices using a step-and-shoot acquisition over 360°. Images were acquired for 40 sec per projection for a total imaging time of approximately 20 min. SPECT images were reconstructed using a filtered backprojection algorithm with a ramp filter after prefiltering with a Butterworth filter (cutoff frequency of 0.25 and order 8.0). A polar map was created using a series of short-axis SPECT images, in which the left ventricle was divided into five segments including the apex, anterior, lateral, inferior and septal walls. Mean counts and washout rates were calculated for each segment and for the entire left ventricle. Physical decay of ^{123}I was not corrected in this study.

Table 1
Subject Data

Subject no.	Age (yr)	Sex	Type of Diabetes	Neuropathy	Duration (yr)	FBS (mg/dl)	HbA1c (%)
1	47	F	Normal	C	·	88	4.9
2	66	F	Normal	C	·	·	·
3	58	F	Normal	C	·	84	4.3
4	44	F	Normal	C	·	99	4.7
5	41	M	Normal	C	·	·	·
6	59	M	Normal	C	·	·	·
7	65	M	Normal	C	·	95	4.9
8	65	M	Normal	C	·	·	·
9	44	M	Normal	C	·	·	·
10	47	M	Normal	C	·	78	4.3
11	59	M	Normal	C	·	·	·
12	47	M	Normal	C	·	97	4.1
13	58	F	NIDDM	N0	0.1	115	5.9
14	48	F	NIDDM	N0	1	256	11.5
15	46	F	NIDDM	N0	10	150	11
16	44	F	NIDDM	N0	6	71	5.6
17	58	F	NIDDM	N0	3	132	6.7
18	58	F	NIDDM	N0	2	103	8.5
19	48	F	NIDDM	N0	4	223	11.3
20	53	M	NIDDM	N0	2	98	7
21	57	M	NIDDM	N0	5	101	6
22	66	M	NIDDM	N0	1	107	8.7
23	48	M	NIDDM	N0	0.25	167	12.5
24	45	M	NIDDM	N0	5	253	11.3
25	61	F	NIDDM	N1	9	105	8.6
26	67	F	NIDDM	N1	12	96	5.5
27	41	F	NIDDM	N1	0.2	156	9.1
28	58	F	NIDDM	N1	16	135	9.5
29	44	M	NIDDM	N1	5	237	10.1
30	69	M	NIDDM	N1	27	127	8.4
31	57	M	NIDDM	N1	23	194	7.9
32	61	M	NIDDM	N1	10	144	6.5
33	61	F	NIDDM	N2	12	158	8.5
34	58	F	NIDDM	N2	25	143	8.8
35	69	F	NIDDM	N2	19	147	11.1
36	60	M	NIDDM	N2	23	198	10.7
37	57	M	NIDDM	N2	22	140	7.7
38	35	M	NIDDM	N2	19	258	7.1
39	64	M	NIDDM	N2	15	74	4.8
40	47	M	NIDDM	N2	11	97	9
41	66	M	NIDDM	N2	20	142	6.4
42	51	M	NIDDM	N2	11	144	8.4
43	36	M	NIDDM	N2	15	148	9.4

*C = without diabetes; N0 = without neuropathy; N1 = mild neuropathy; N2 = severe neuropathy; FBS = fasting blood sugar.

Data Processing

Quantitative indices of MIBG can be divided into three categories: (a) global uptake, (b) washout rates and (c) regional distribution. For global uptake indices, we evaluated as the myocardial uptake ratio of MIBG and the heart-to-mediastinum count ratio. For washout indices, we evaluated the washout rate in the inferior wall (WR(inferior)) and the entire left ventricle (WR(total)). For indices of regional distribution, we evaluated the inferior-to-anterior count ratio and the coefficient of variation of MIBG uptake.

Global MIBG Uptake

The myocardial uptake ratio of MIBG was calculated using dynamic planar as well as planar image data as previously reported (*15,16*). The concept of the uptake ratio (UR) is expressed as:

UR = count of the heart/total injected dose of MIBG. Eq. 1

The total injected dose was obtained from the peak counts of the entire field of view during dynamic planar imaging.

We also used another method to quantify global cardiac MIBG uptake by obtaining the heart-to-mediastinum ratio from early and late planar images, placing the regions of interest (ROIs) over the heart and upper mediastinum, respectively (*17*).

Regional MIBG Uptake and Washout Rate

As an index of regional MIBG uptake, the inferior-to-anterior count ratio was calculated as the mean counts of the inferior segment divided by those of the anterior segment. The coefficient of variation was calculated as the standard deviation of the entire left ventricle divided by the mean value, as a marker of heterogeneity of MIBG distribution. The washout rates were calculated as:

$$WR = (\text{early count} - \text{late count})/\text{early count} \times 100\ (\%). \quad \text{Eq. 2}$$

Statistical Analysis

All data are expressed as mean ±1 s.d. The difference among groups (C, N0-N2) were analyzed for variance by calculating the F-ratio from ANOVA tables followed by intergroup comparisons with Scheffe's F-test. A value of $p < 0.05$ was considered significant.

RESULTS

Detection of Diabetes by MIBG Imaging

In the detection of diabetes in the three groups (N0, N1 and N2), both the planar and SPECT images of the late phase data showed higher sensitivity and specificity than the early phase data. SPECT images showed better sensitivity, although specificity was almost the same for both types of imaging studies. Overall sensitivity/specificity of the planar images was 20%/80% for early image data and 37%/100% for late image data. Sensitivity/specificity values for the SPECT images were 60%/92% for early image data and 80%/92% for late image data.

Pattern of MIBG Abnormality

MIBG abnormalities were observed to be heterogeneous. In Group N0, a slight reduction was seen only in the inferior wall. It spread to the adjacent segments and became more severe along with clinical presentation of diabetic neuropathy (Fig. 1).

Quantitative Analysis

Radiopharmaceutical data and the result of one-factor ANOVA are summarized in Table 2. In the early phase data, significant differences were observed in the inferior-to-anterior ratios and the coefficient of variation. In the late phase data, significant differences were observed in heart-to-mediastinum and inferior-to-anterior ratios and in the coefficient of variation. Heart-to-mediastinum ratios (early image), MIBG uptake ratios (early, late images) and washout rates (total, inferior) did not show significant differences.

The heart-to-mediastinum (late) values for Groups N1 and N2 were smaller than those for Groups C and N0, but intergroup comparison using Scheffe's F-test showed no significant difference between any pair of groups.

Washout rates tended to be higher with progression of diabetic neuropathy from Groups N0 to N2, particularly in the inferior wall. However, intergroup comparison revealed no significant difference, even between Groups C and N2 (Fig. 2).

All regional indices showed significant differences by ANOVA. Inferior-to-anterior ratios (early image) decreased with diabetic neuropathy. Intergroup comparison showed significant differences between Groups C–N1 and N1–N2 ($p < 0.05$). Inferior-to-anterior ratios (late image) also decreased with the progression of diabetic neuropathy: significant differences were observed between Groups C–N1 ($p < 0.01$) and N1–N2 ($p < 0.05$) (Fig. 3).

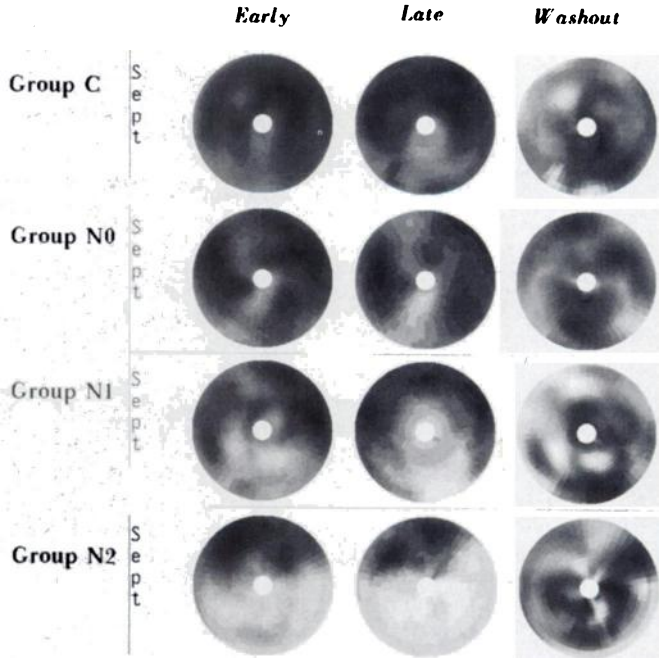

FIGURE 1. Polar map displays of typical subject in each group. First row: control group (C). Second row: diabetes without neuropathy (Group N0). Third row: diabetes with mild neuropathy (Group N1). Fourth row: diabetes with severe neuropathy (Group N2). MIBG abnormality was obvious in the inferior segment and became more severe, spreading to the adjacent segments with diabetic neuropathy (left and middle columns). Washout rate was enhanced in the inferior wall (right column).

The coefficient of variation values (early, late images) as a marker of regional heterogeneity of MIBG uptake increased with diabetic neuropathy. Intergroup comparison showed that the coefficient of variation (early image) for Group N2 was significantly greater than those of the other groups. Due to the greater standard deviation, the coefficient of variation (late image) showed a significant difference only between Groups C and N2 ($p < 0.05$).

DISCUSSION

The results of the present study indicate that diabetic neuropathy involves an MIBG abnormality even in its early stages. The abnormality initially appears in the inferior wall and then gradually spreads to the adjacent segments as it advances. Thus, in the early stages of diabetic neuropathy, only regional distribution indices of MIBG showed abnormal values, while global uptake indices remained within the normal ranges. Of the regional indices, the inferior-to-anterior count ratio is considered to be suitable for evaluating cardiac denervation because of its superior sensitivity and clearer relationship with the severity of diabetic neuropathy. Our study also clarified that washout of MIBG was enhanced in the inferior wall where cardiac denervation was observed.

Regional Denervation Precedes Global Denervation

Although diabetes is a metabolic disorder affecting every system in the human body, the present study proves that the cardiac MIBG abnormality occurrs heterogeneously, starting in the inferior segment and spreading to the adjacent segments with the progression of neuropathy. Thus, cardiac denervation was present only in the inferior segment during early stages. Previous studies demonstrated significant MIBG abnormalities or ^{11}C-hydroxyephedrine uptake in patients with advanced

Table 2
Summary of the Results

Category	MIBG	Without diabetes	Diabetic patients			ANOVA	
		C	N0	N1	N2	F-ratio	p value
Global uptake	H/M (early)	2.61 ± 0.46	2.74 ± 0.36	2.45 ± 0.19	2.42 ± 0.44	1.63	ns (p = 0.21)
	H/M (late)	2.82 ± 0.59	2.92 ± 0.45	2.30 ± 0.36	2.39 ± 0.56	3.69	p = 0.02
	n = 43						
	UR (early)	0.54 ± 0.19	0.70 ± 0.23	0.78 ± 0.14	0.54 ± 0.24	1.94	ns (p = 0.15)
	UR (late)	0.52 ± 0.17	0.64 ± 0.18	0.34 ± 0.17	0.47 ± 0.34	1.77	ns (p = 0.17)
	n = 33						
Washout rate	WR (total)	25.4 ± 8.63	28.7 ± 9.62	35.7 ± 8.01	35.6 ± 18.4	1.95	ns (p = 0.14)
	WR (inferior)	27.9 ± 9.27	31.7 ± 9.85	37.5 ± 9.35	42.4 ± 20.2	2.68	ns (p = 0.06)
	n = 43						
Regional distribution	I/A (early)	0.91 ± 0.11	0.85 ± 0.10	0.75 ± 0.12	0.58 ± 0.10	20.8	p < 0.0001
	I/A (late)	0.84 ± 0.10	0.79 ± 0.12	0.66 ± 0.13	0.47 ± 0.11	22.8	p < 0.0001
	n =43						
	CV (early)	0.11 ± 0.02	0.12 ± 0.04	0.17 ± 0.05	0.29 ± 0.07	34.1	p < 0.0001
	CV (late)	0.13 ± 0.03	0.33 ± 0.34	0.44 ± 0.34	0.52 ± 0.24	4.76	p < 0.01
	n = 43						

Data are expressed as mean ± s.d.

C = without diabetes; N0 = without neuropathy; N1 = mild neuropathy; N2 = severe neuropathy; H/M = heart-to-mediastinum count ratio; UR = uptake ratio; WR = washout ratio; I/A = inferior-to-anterior count ratio; CV = coefficient of variation; ns = not significant.

diabetic neuropathy. These studies, however, failed to detect the minimal denervation seen only in the early stages (*9,18*). The most likely reason for this is that the conventional quantitative indices were not sensitive enough to detect the slight reduction of MIBG. In our study, the widely used index, heart-to-mediastinum ratio, actually showed less sensitivity compared with the indices of regional uptake. This ratio may be helpful in detecting severe neuropathy. However, it may not be useful for evaluating the severity of denervation due to diabetes. Given that diabetic neuropathy is reversible if treated in the early stages (*19,20*), early detection is very important to achieve a better prognosis.

Possible Mechanism of Regional Heterogeneity

The pathophysiology of this condition still remains unclear. Proposed mechanisms of neural damage include metabolic abnormalities, neuronal ischemia and immune-mediated injury. Previous studies demonstrated that the anterior and inferior walls each have a different supply of sympathetic and parasympathetic innervation (*21,22*), and this may account for the regional heterogeneity.

The characteristic pattern of diabetic neuropathy may also account for this condition. In diabetic patients, peripheral neuronal damage starts in the most distal sites. A similar length-dependent pattern may be seen in cardiac sympathetic nerve terminals, and denervation starts from the most distal site (apex), spreading to the proximal site (base). The inferior wall may be relatively distal to the anterior wall in sympathetic supply. The anatomical distribution of sympathetic nerve supply is still unclear as is the mechanism of denervation. Further study is warranted to explain these findings.

Artifacts resulting from relatively high hepatic activity should also be considered. Kobayashi et al. (*23*) reported that relatively low cardiac activity to the liver caused count reduction in the inferior cardiac wall. However, our phantom study confirmed the effect only in the 180° data collection method with high hepatic positioning. The effect was not seen in the

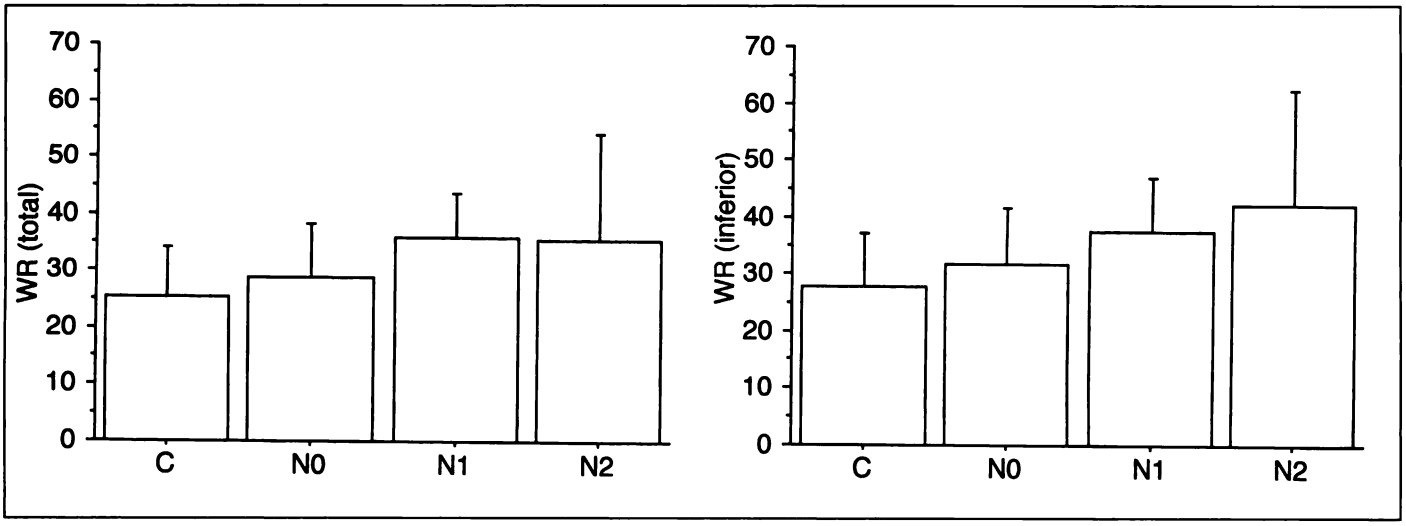

FIGURE 2. MIBG washout rate (WR) increased as diabetic neuropathy progressed. Inferior wall (WR (inferior); right) had greater washout, in which regional MIBG distribution showed an obvious abnormality.

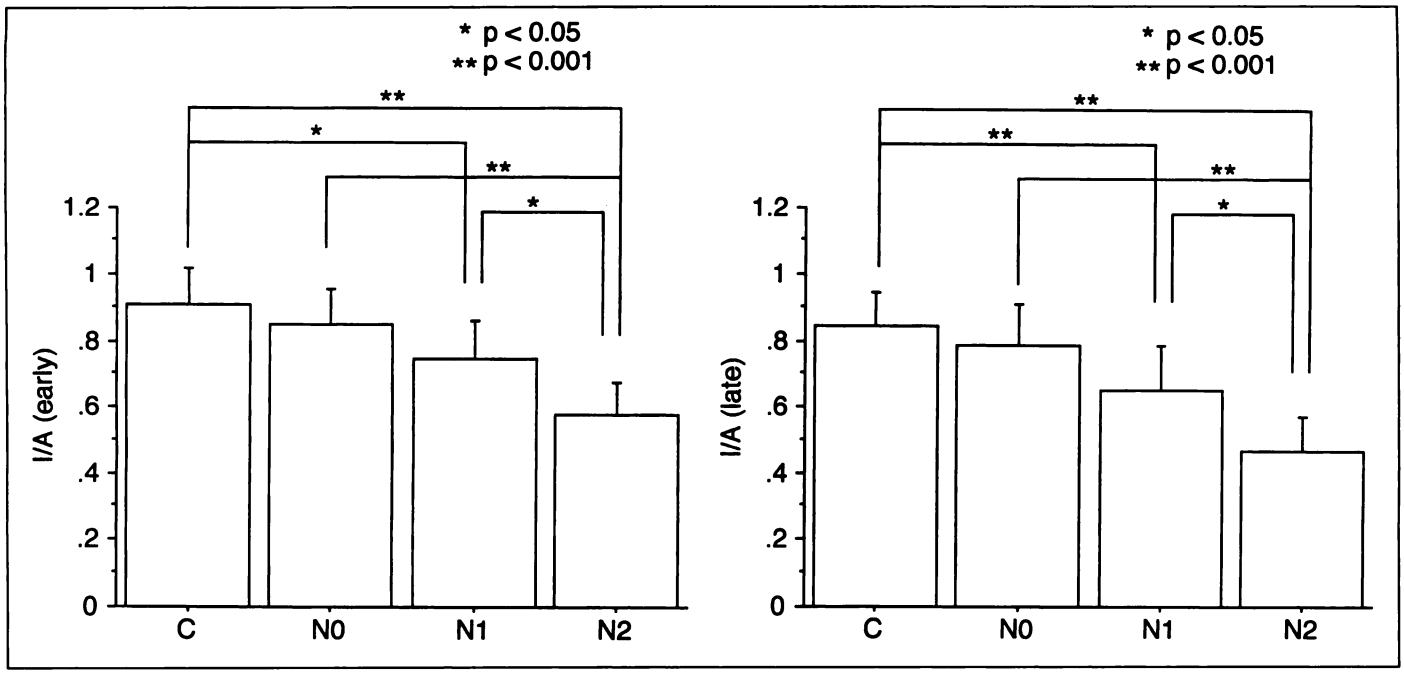

FIGURE 3. Inferior-to-anterior count ratio (I/A). Data were obtained from early and late SPECT images. I/A values decreased with diabetic neuropathy. Intergroup comparison demonstrated significant differences (*$p < 0.05$, **$p < 0.001$).

360° data collection method used in our study. Our findings correlated with Kobayashi et al., in that 360° data collection is more desirable to avoid this artifact.

MIBG Washout

Although the difference was not significant among groups (C, N0-N2), MIBG washout of the inferior segment tended to increase with the progression of neuropathy. In diabetic cardiomyopathy, an increase in sympathetic activity was reported by Ganguly et al. (*20*) in pharmacologically-induced diabetes in rats. These observations may explain the mechanism of enhanced washout rate in the inferior segment. In the inferior segment with reduced sympathetic nerve terminals, the remaining nerves may be activated to compensate for the loss of quantity. This explanation is compatible with published reports indicating that sympathetic denervation was seen even in hearts without left ventricular dysfunction at rest (*10,24*). In the resting condition, denervation may be well compensated for increased sympathetic tone, resulting in normal ventricular function. However, the compensation capacity may be decreased in such hearts and may show dysfunction with exercise stress. This phenomenon was reported by Kreiner et al. (*11*) who demonstrated paradoxical decrease of left ventricular ejection fraction (LVEF) during exercise in IDDM patients with reduced MIBG uptake.

Future Implications

Cardiac denervation occurs heterogeneously in diabetic patients. From this point of view, cardiac function and metabolism should be studied on a regional basis. Even if global cardiac function is normal, diabetic hearts may show regional dysfunction, particularly in the inferior region, because the quantity of norepinephrine released by sympathetic nerve endings in the heart is the most important factor regulating myocardial contractility under physiological conditions. Further studies should be conducted to assess cardiac function and metabolsim regionally to better understand the pathophysiology of diabetic autonomic neuropathy.

CONCLUSION

Diabetic neuropathy involves an MIBG abnormality in its early stages. The abnormality first occurred in the inferior wall and became more severe with neuropathic progression. The inferior-to-anterior count ratio may be a suitable index for evaluating diabetic neuropathy because of its superior sensitivity.

ACKNOWLEDGMENTS

We thank Toru Fujita and Jinyi Wang for technical assistance.

REFERENCES

1. Ewing DJ, Cambell IW, Clarke BF. The natural history of diabetic autonomic neuropathy. *Q J Med* 1980;49(193):95–108.
2. Sisson JC, Shapiro B, Meyers L, et al. Metaiodobenzylguanidine to map scintigraphically the adrenergic nervous system in man. *J Nucl Med* 1987;28:1625–1636.
3. Ewing DJ, Campbell IW, Clarke BF. Assessment of cardiovascular effects in diabetic autonomic neuropathy and prognostic implications: II. *Ann Intern Med* 1980;92:308–311.
4. Pfeifer MA, Cook D, Brodsky J, et al. Quantitative evaluation of cardiac parasympathetic activity in normal and diabetic man. *Diabetes* 1982;31:339–345.
5. Ewing DJ, Martyn CN, Young RJ, Clarke BF. The value of cardiovascular autonomic function tests: 10 yr experience in diabetes. *Diabetes Care* 1985;8:491–498.
6. Freeman R, Saul JP, Roberts MS, Berger RD, Broadbridge C, Cohen RJ. Spectral analysis of heart rate in diabetic autonomic neuropathy. A comparison with standard tests of autonomic function. *Arch Neurol* 1991;48:185–190.
7. Lishner M, Akselrod S, Avi VM, Oz O, Divon M, Ravid M. Spectral analysis of heart rate fluctuations: a noninvasive, sensitive method for the early diagnosis of autonomic neuropathy in diabetes mellitus. *J Auton Nerv Syst* 1987;19:119–125.
8. Jaques S Jr., Tobes MC, Sisson JC, Baker JA, Wieland DM. Comparison of the sodium dependency of uptake of meta-iodobenzylguanidine and norepinephrine into cultured bovine adrenomedullary cells. *Mol Pharmacol* 1984;26:539–546.
9. Mantysaari M, Kuikka J, Mustonen J, et al. Noninvasive detection of cardiac sympathetic nervous dysfunction in diabetic patients using [^{123}I]metaiodobenzylguanidine. *Diabetes* 1992;41:1069–1075.
10. Langer A, Freeman MR, Josse RG, Armstrong PW. Metaiodobenzylguanidine imaging in diabetes mellitus: assessment of cardiac sympathetic denervation and its relation to autonomic dysfunction and silent myocardial ischemia. *J Am Coll Cardiol* 1995;25:610–618.
11. Kreiner G, Wolzt M, Fasching P, et al. Myocardial *m*-^{123}I-iodobenzylguanidine scintigraphy for the assessment of adrenergic cardiac innervation in patients with IDDM. Comparison with cardiovascular reflex tests and relationship to left ventricular function. *Diabetes* 1995;44:543–549.
12. Tsuchimochi S, Tamaki N, Tadamura E, et al. Age and gender differences in normal myocardial adrenergic neuronal function evaluated by iodine-123-MIBG imaging. *J Nucl Med* 1995;36:969–974.
13. Tsuchimochi S, Tamaki N, Shirakawa S, et al. Evaluation of myocardial distribution of iodine-123-labeled metaiodobenzylguanidine (^{123}I-MIBG) in normal subjects. *Kaku Igaku* 1994;31:257–264.

14. Yamasaki Y, Ueda N, Kishimoto M, et al. Assessment of early stage autonomic nerve dysfunction in diabetic subjects-application of power spectral analysis of heart rate variability. *Diabetes Res* 1991;17:73-80.
15. Yonekura Y, Ishii Y, Torizuka K, Kadota K, Kambara H, Kawai C. Quantitative assessment of myocardial blood flow by measurement of fractional myocardial uptake of ^{201}Tl. *Kaku Igaku* 1980;17:1211-1220.
16. Peters AM. A unified approach to quantification by kinetic analysis in nuclear medicine. *J Nucl Med* 1993;34:706-713.
17. Merlet P, Valette H, Dubois-Rande JL, et al. Prognostic value of cardiac metaiodobenzylguanidine imaging in patients with heart failure [see comments]. *J Nucl Med* 1992;33:471-477.
18. Allman KC, Stevens MJ, Wieland DM, et al. Noninvasive assessment of cardiac diabetic neuropathy by carbon-11-hydroxyephedrine and positron emission tomography. *J Am Coll Cardiol* 1993;22:1425-1432.
19. Brismar T, Sima AA, Greene DA. Reversible and irreversible nodal dysfunction in diabetic neuropathy. *Ann Neurol* 1987;21:504-507.
20. Ganguly PK, Beamish RE, Dhalla KS, Innes IR, Dhalla NS. Norepinephrine storage, distribution and release in diabetic cardiomyopathy. *Am J Physiol* 1987;252:E734-E739.
21. Yoran C, Higginson L, Romero MA, Covell JW, Ross J Jr. Reflex sympathetic augmentation of left ventricular inotropic state in the conscious dog. *Am J Physiol* 1981;241:H857-H863.
22. Thames MD, Klopfenstein HS, Abboud FM, Mark AL, Walker JL. Preferential distribution of inhibitory cardiac receptors with vagal afferents to the inferoposterior wall of the left ventricle activated during coronary occlusion in the dog. *Circ Res* 1978;43:512-519.
23. Kobayashi H, Terada S, Kanaya S, et al. Artifactual defect of inferior myocardium on ^{123}I-metaiodobenzylguanidine myocardial SPECT: characteristic findings and preventive method on phantom study. *Kaku Igaku* 1994;31:359-366.
24. Wakasugi S, Fischman AJ, Babich JW, et al. Metaiodobenzylguanidine: evaluation of its potential as a tracer for monitoring doxorubicin cardiomyopathy. *J Nucl Med* 1993;34:1283-1286.

Simultaneous Evaluation of Fatty Acid Metabolism and Myocardial Flow in an Explanted Heart

Margot Jonas, Wolfgang Brandau, Bernhard Vollet, Michael Weyand, Anke Fahrenkamp, Franz-Josef Gildehaus, Joachim Sciuk, Hans H. Scheld and Otmar Schober

Departments of Nuclear Medicine, Cardiothoracic Surgery and Pathology, Westfälische Wilhelms University of Münster, Münster, Germany

The biodistribution of the fatty acid analog [^{131}I]PHIPA 3–10, was compared to the flow tracer ^{99m}Tc-sestamibi by quantitative analysis in a dual-isotope study performed during a heart transplantation. **Methods:** Iodine-131-PHIPA 3–10 and ^{99m}Tc-sestamibi were injected simultaneously approximately 20 min prior to the start of surgical procedure. Scintigraphic images of the sliced explanted heart were compared to the preoperative in vivo scans using [^{123}I]PHIPA 3–10, ^{201}Tl and ^{99m}Tc-sestamibi. In 14 tissue samples of the explanted heart, the radioactive contents from [^{131}I]PHIPA 3–10 and ^{99m}Tc-sestamibi were calculated as %ID/g-values and correlated with the corresponding histology. **Results:** In the preoperative scans, a mismatch of fatty acid uptake and perfusion ([^{123}I]PHIPA 3–10 > flow) was observed which indicated residual viable myocardium, while a matched defect was associated with scar. In viable myocardium, there was a significantly higher accumulation of [^{131}I]PHIPA 3–10 compared to ^{99m}Tc-sestamibi (mean 5.9×10^{-3} versus 2.7×10^{-3} %ID/g), whereas in scars the uptake of both tracers was comparable (1.2×10^{-3} versus 1.4×10^{-3} %ID/g). **Conclusion:** Myocardial viability can be defined more accurately with radioiodinated PHIPA 3–10 than with ^{99m}Tc-sestamibi. The differences of biodistribution in viable myocardium and scars indicate that not only perfusion but also the metabolic state of the myocardium can be evaluated with radioiodinated PHIPA 3–10.

Key Words: myocardial viability; iodine-123 fatty acid; dual-isotope study; pathology; heart transplantation

J Nucl Med 1996; 37:1990–1994

The detection of residual viable myocardium is an important factor in deciding whether to perform percutaneous transluminal coronary angioplasty (PTCA) or coronary bypass graft surgery (CABG). In many experimental and clinical trials, the use of radioiodinated free fatty acids (FFA) for assessment of myocardial viability has been elucidated (*1–4*). For enhancement of myocardial retention, various FFA analogs have been developed to inhibit rapid fatty acid catabolism by beta-oxidation (*5*). Most experience has been obtained with p-^{123}I-phenylpentadecanoic acid (p-IPPA) and p-^{123}I-β-methyl-IPPA (BMIPP) recently available in Japan (*1,2*).

Phenylene-bridged long-chain fatty acid analogs offer an alternative approach to methyl-branching to delay myocardial clearance and were first described by Liefhold and Eisenhut in 1987 and 1988 (*6,7*). In contrast to many other fatty acid analogs, [^{123}I]-PHIPA 3–10 (13-(p-[^{123}I]iodophenyl]-3-(p-phenylene)-tridecanoic acid) (Fig. 1) has a prolonged biological half-life in human myocardium (>15 hr), indicating metabolic trapping and is therefore more suited for SPECT investigations than unmodified phenyl fatty acids (*8–10*).

The aim of this study was to simultaneously examine [^{131}I]PHIPA 3–10 biodistribution compared to perfusion in the human myocardium. Myocardial accumulation of [^{131}I]PHIPA 3–10 and ^{99m}Tc-sestamibi was thus quantified in a dual-isotope study performed during heart transplantation. Distribution patterns and scintigraphic images of the heart in vivo and ex vivo were correlated to histological examination of the explanted heart.

MATERIALS AND METHODS

Radiopharmaceuticals

Iodine-123 and [^{131}I]PHIPA 3–10 were labeled by a non-carrier-added Cu(I)-assisted, nonisotopic halogen exchange (*11*). Briefly, ^{123}I or ^{131}I-sodium iodide were evaporated to dryness followed by the addition of the bromo-precursor and 5 μl of a CuCl solution (1 mg/ml acetic acid). After heating for 10 min at 180°C, the residue was dissolved in 200 μl absolute ethanol and purified by means of HPLC. The eluate was evaporated to dryness, dissolved in 150 μl ethanol, added dropwise to 10 ml of a solution of 5% human serum albumin and then filtered (0.22 μm). Thallium-201 and ^{99m}Tc-sestamibi were both commercially obtained.

Received Dec. 12, 1995; revision accepted Apr. 4, 1996.

For correspondence or reprints contact: Margot Jonas, MD, Department of Nuclear Medicine, Westfälische Wilhelms-Universität Münster, Albert-Schweitzer-Strasse 33, D-48129 Münster, Germany.